

# Measured Instantaneous Viscous Boundary Layer in Turbulent Rayleigh-Bénard Convection

Quan Zhou<sup>1,2</sup> and Ke-Qing Xia<sup>1</sup>

<sup>1</sup>*Department of Physics, The Chinese University of Hong Kong, Shatin, Hong Kong, China*

<sup>2</sup>*Shanghai Institute of Applied Mathematics and Mechanics, Shanghai University, Shanghai 200072, China*

(Dated: September 12, 2018)

We report measurements of the instantaneous viscous boundary layer (BL) thickness  $\delta_v(t)$  in turbulent Rayleigh-Bénard convection. It is found that  $\delta_v(t)$  obtained from the measured instantaneous two-dimensional velocity field exhibits intermittent fluctuations. For small values,  $\delta_v(t)$  obeys a lognormal distribution, whereas for large values the distribution of  $\delta_v(t)$  exhibits an exponential tail. The variation of  $\delta_v(t)$  with time is found to be driven by the fluctuations of the large-scale mean flow velocity and the local horizontal velocities close to the plate can be used as an instant measure of this variation. It is further found that in the present parameter range of the experiment the mean velocity profile measured in the laboratory frame can be brought into coincidence with the theoretical Prandtl-Blasius laminar BL profile, if it is resampled relative to the time-dependent frame of  $\delta_v(t)$ .

PACS numbers: 44.25.+f, 44.20.+b, 47.27.-i

An important issue in the study of fluid dynamics is to determine the velocity within a very thin layer in the neighborhood of the plates and walls, i.e. the viscous boundary layer (BL) [1]. The classical Prandtl-Blasius BL, derived more than 100 years ago for flows over a flat plate, remains one of the few BLs with exact theoretical profile based on the equations of motion. For turbulent boundary layers, the well-known, empirical, logarithmic “law of wall” can be used to describe the shape of the velocity profile near the boundary. However, there are situations in which the BL is neither fully turbulent nor strictly laminar, but fluctuates with time. How to characterize such BLs quantitatively has long been a challenge. Here, we present a method that expresses the measured boundary layer quantities in a time-dependent frame that fluctuates with the boundary layer thickness. We use the turbulent Rayleigh-Bénard (RB) convection as the test case and show that the mean velocity profile measured in the laboratory frame can be brought into coincidence with the theoretical Prandtl-Blasius laminar BL profile, if it is resampled relative to the time-dependent frame of BL thickness. More generally, the concept and the algorithm presented in this work may serve as an example on how to disentangle the mixed dynamics in quantities from local measurements.

The Rayleigh-Bénard system has become a paradigm for the study of general convection phenomena occurring in nature [2]. There already exist a number of studies of the viscous BL in RB convection [3–11], however, an important issue remains unresolved. Scaling wise and in a time averaged sense, it has been found that the measured BL properties are the same as those of the Prandtl-Blasius-type laminar BL [2, 6, 11]. Whereas, the time-averaged velocity profile is found to differ from both the Prandtl-Blasius-type laminar BL and the turbulent log-

arithmic BL [10], especially for the region around the thermal BL where thermal plumes are generated. We note that, as the viscous BL is produced and stabilized by the viscous shear of the large-scale mean flow, the fluctuations of the large-scale velocity would cause the viscous BL to fluctuate as well, which would in turn cause a fixed measurement point to be sometimes inside and sometimes outside the BL [11]. In this respect, the time-averaged properties are not sufficient to reveal the dynamic nature of the BL. As fluctuating BLs exist in various flow systems, a more effective analysis method is thus highly desirable to unlock the intricate flow dynamics in the vicinity of plates, which is the objective of the present work.

Two water-filled rectangular cells were used in the experiments, the details of which have been described elsewhere [12]. The length, width, and height, in unit of cm, of the small cell are  $25 \times 7 \times 24$  and those of the large cell are  $81 \times 20 \times 76$ . The experiment was conducted at fixed Prandtl number  $\text{Pr} = 4.3$ . The small-cell measurements covered the range  $10^9 \lesssim \text{Ra} \lesssim 2 \times 10^{10}$  of the Rayleigh number  $\text{Ra}$  and the large-cell measurements were made in the regime  $2 \times 10^{10} \lesssim \text{Ra} \lesssim 7 \times 10^{11}$ . The technique of particle image velocimetry (PIV) was used to measure the velocity fields above the center of the bottom plate and within the vertical circulation plane of the large-scale mean flow. The measuring region for the large (small) cell experiments has an area of  $17.2 \times 21.5$  ( $11.1 \times 13.8$ )  $\text{mm}^2$ , corresponding to  $63 \times 79$  velocity vectors, with a spatial resolution 0.27 (0.17) mm. The large (small) cell measurement for each  $\text{Ra}$  lasted 4.42 (3.79) hours in which a total of 35000 (30000) vector maps were acquired at a sampling rate  $\sim 2.2$  Hz. The time-averaged statistical properties and various scaling behaviors of the viscous BL measured in the small cell have been reported

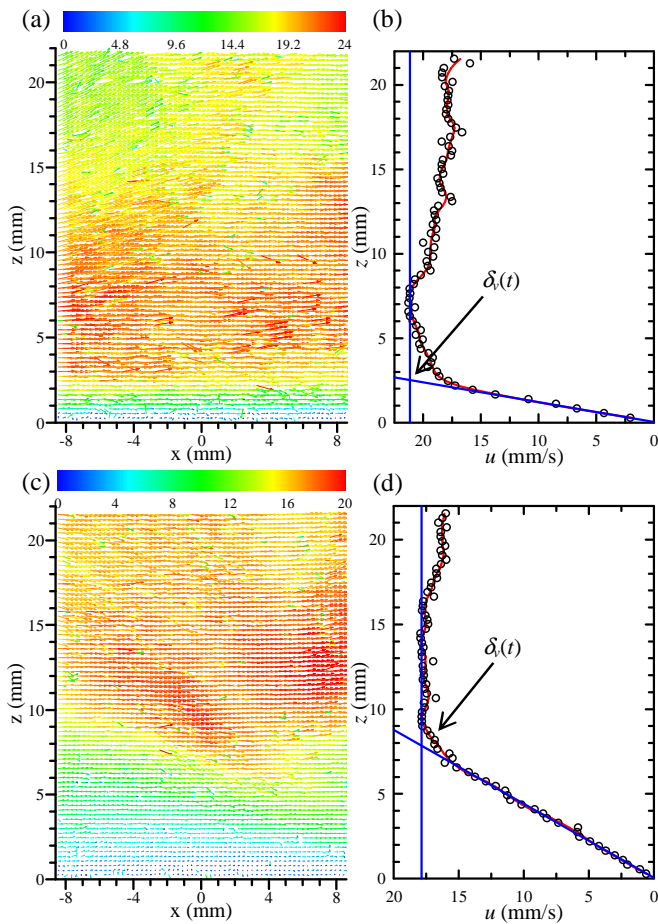


FIG. 1: (color online) (a, c) Two examples of the instantaneous velocity fields measured near the center of the bottom plate ( $Ra = 1.9 \times 10^{11}$ ). (b, d) The horizontal velocity profiles  $u(z, t)$  corresponding to those in (a) and (c), but averaged over  $-2 \text{ mm} \leq x \leq 2 \text{ mm}$ . The magnitude of the velocity in (a,c) is coded in both color scale and the length of the arrows in unit of mm/s. The solid lines in (b,d) illustrate how  $\delta_v(t)$  is obtained.

previously [11]. Here we make new analysis to the data and present the results alongside with those from the new measurements in the large cell.

Figures 1(a) and 1(c) show two examples of the instantaneous velocity fields. It is seen that the velocity fields near the plate show strong fluctuations and larger velocity magnitude yields thinner viscous BL. To obtain more quantitative information, we calculate this fluctuating BL thickness from the instantaneous velocity field using the following procedure. To reduce data scatter, we first coarse grain the measured velocity field by averaging it along the  $x$ -direction over a range of 2 mm for the small cell and 4 mm for the large cell. This yields the horizontal velocity profile  $u(x, z, t)$  at time  $t$ . As the profile shows only weak  $x$ -dependence, we will hereafter present and discuss results measured at the center of the plate, i.e.  $u(z, t) \equiv u(0, z, t)$  [circles in Figs. 1(b) and

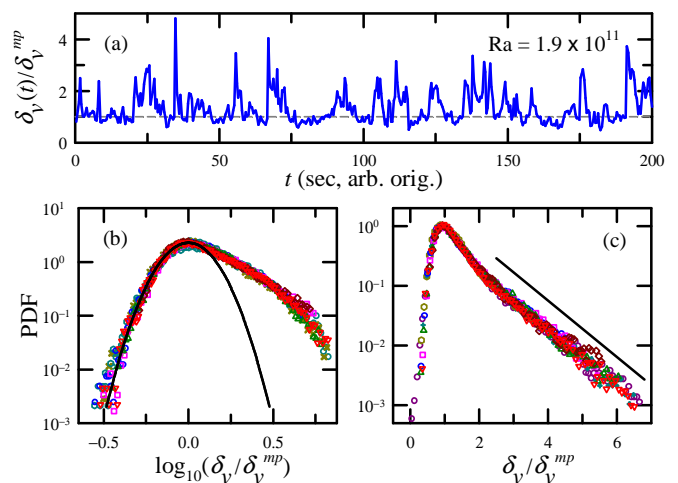


FIG. 2: (color online) (a) A sample time trace of instantaneous viscous BL thickness  $\delta_v(t)$ , normalized by its most-probable value  $\delta_v^{mp}$ . (b) PDFs of  $\log_{10}(\delta_v/\delta_v^{mp})$  and (c) those of  $\delta_v/\delta_v^{mp}$  measured at various  $Ra$  varying from  $1.25 \times 10^9$  to  $6.4 \times 10^{11}$ . The solid curve in (b) marks the lognormal distribution for reference.

1(d)]. Next, to increase the statistical accuracy, each profile is smoothed by using the locally weighted scatterplot smoothing method [13], denoted as  $u_s(z, t)$  [solid curves in Figs. 1(b) and 1(d)]. A linear fitting is then made to  $u_s(z, t)$  close to the plate. Denote the maximum velocity of  $u_s(z, t)$  as  $u_m(t)$ , the instantaneous viscous BL thickness  $\delta_v(t)$  is then obtained as the distance from the plate at which the extrapolation of the linear fitting of  $u_s(z, t)$  crosses  $u_m(t)$ . The uncertainty of  $\delta_v(t)$ , primarily due to uncertainties of  $u_m(t)$  and the linear fitting to  $u_s(z, t)$  close to the plate, is estimated to be about 3%. We note that the results are robust and insensitive to the algorithm used to smooth the profile.

Figure 2 shows a 200-second time trace of  $\delta_v(t)$ , normalized by the most-probable thickness  $\delta_v^{mp}$ . One sees that the fluctuating  $\delta_v(t)$  exhibits intermittent features, i.e., the amplitude of  $\delta_v(t)$  can be much larger than its mean or most-probable value. We find that, for all measured values of  $Ra$ ,  $\delta_v^{mp}$  coincides with the viscous BL thickness  $\lambda_v$  (to within 4%) [11], defined through the slope of the time-averaged velocity profile at the plates that have been previously studied extensively. The probability density functions (PDF) of  $\log_{10}(\delta_v/\delta_v^{mp})$  and  $\delta_v/\delta_v^{mp}$  are plotted in Figs. 2(b) and 2(c) respectively. For either PDF there is reasonable collapse for all measured  $Ra$  from both cells, which suggests a universality of the BL dynamics in turbulent RB system. In addition, it is seen that the tails of the PDFs at large  $\delta_v$  ( $> \delta_v^{mp}$ ) can be described by a decaying exponential distribution, whereas those at small  $\delta_v$  ( $\lesssim \delta_v^{mp}$ ) satisfy a lognormal statistics. The mechanism that leads to the different distributions of  $\delta_v$  below and above its most probable

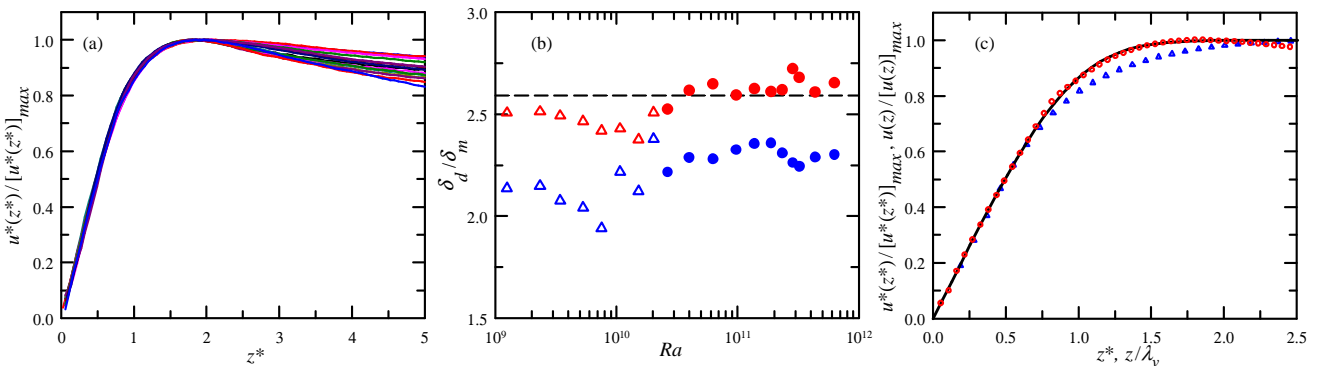


FIG. 3: (color online) (a) Normalized profiles of  $u^*(z^*)$  for all measured  $Ra$  ranging from  $1.25 \times 10^9$  to  $6.4 \times 10^{11}$ . (b) The shape factors  $\delta_d/\delta_m$  of  $u^*(z^*)$  (red symbols) and  $u(z)$  (blue symbols) vs.  $Ra$  for the small-cell (open triangles) and large-cell (solid circles) data. The dashed line represents the value of 2.59 for the Prandtl-Blasius BL. (c) Comparison among several velocity profiles:  $u^*(z^*)$  (red circles),  $u(z)$  (blue triangles), and the Prandtl-Blasius profile (black line). The data were measured at  $Ra = 1.9 \times 10^{11}$ .

values is at present unknown and would be a challenge for future theoretical studies. However, it is clear that measurement made at a fixed position in the laboratory frame and near the boundary layer will sample a mixed statistic (one pertaining to the boundary layer and the other pertaining to the bulk), because that position will be sometimes inside and sometimes outside of the fluctuating BL. To achieve a clean separation of the two types of dynamics in the measured velocity, we define the time-dependent relative vertical position  $z^*(t)$  with respect to  $\delta_v(t)$ , i.e.,

$$z^*(t) = z/\delta_v(t), \quad (1)$$

and hence  $z^*$  is the rescaled distance from the plate in unit of BL thickness. The mean velocity profile  $u^*(z^*)$  in this time-dependent frame is then calculated by averaging all values of  $u(z, t)$  that were measured at different discrete time  $t$  but at the same relative position  $z^*$ , i.e.,

$$u^*(z^*) = \langle u(z, t) | z = z^*\delta_v(t) \rangle. \quad (2)$$

The results are shown in Fig. 3(a), normalized by the maximum value of each profile  $[u^*(z^*)]_{max}$ . One sees excellent collapse of all profiles for the regions inside and around the viscous BL ( $z^* \lesssim 2$ ), suggesting a universal BL profile for all  $Ra$  measured in the two cells. For comparison, we also calculate the time-averaged velocity  $u(z) = \langle u(z, t) \rangle$  for each fixed position  $z$ . We note that  $u^*(z^*)$  is more universal than  $u(z)$  in the sense that profiles for different values of  $Ra$  collapse better in the time-dependent frame than they do in the laboratory frame.

To characterize the shape of the  $u^*(z^*)$  profile more quantitatively, we examine its shape factor  $\delta_d/\delta_m$ , where

$$\delta_d = \int_0^\infty \left\{ 1 - \frac{u^*(z^*)}{[u^*(z^*)]_{max}} \right\} dz^* \quad (3)$$

and

$$\delta_m = \int_0^\infty \left\{ 1 - \frac{u^*(z^*)}{[u^*(z^*)]_{max}} \right\} \left\{ \frac{u^*(z^*)}{[u^*(z^*)]_{max}} \right\} dz^* \quad (4)$$

are the displacement thickness and the momentum thickness, respectively [1]. Because of the zero mean-flow in the central region of a closed convection cell [12],  $u^*(z)$  decays after reaching its maximum value and hence the above integrations are evaluated only over the range from  $z^* = 0$  to where  $u^*(z^*) = [u^*(z^*)]_{max}$ . For comparison, we also show the shape factors of the  $u(z)$  profiles measured in the laboratory frame, which are represented by blue symbols in Fig. 3(b). It is seen that for all values of  $Ra$ ,  $\delta_d/\delta_m$  of  $u(z)$  are clearly smaller than 2.59 — the value of a Prandtl-Blasius laminar BL profile. This is because the time-averaged BL quantities obtained in the laboratory frame are contaminated by contributions from the bulk that has a different dynamics. It is also seen that the shape factors of  $u^*(z^*)$  (red symbols), measured in the time-dependent frame, are much closer to the Prandtl-Blasius value. This suggests that the algorithm using the dynamical coordinates can effectively disentangle the mixed dynamics inside and outside the fluctuating BLs. To see this more clearly, we directly compare in Fig. 3(c) the velocity profiles  $u^*(z^*)$  (circles) and  $u(z)$  (triangles), based on the same data set ( $Ra = 1.9 \times 10^{11}$ ) but measured in the time-dependent and laboratory frames respectively, with the theoretical Prandtl-Blasius profile (solid line) [1]. Here, to make a proper comparison, the initial slope of the Prandtl-Blasius profile is matched to that of the measured profiles by adjusting the path length  $x_0$  in the similarity parameter  $\eta = z\sqrt{u_{max}/2x_0\nu}$  [10]. ( $\nu$  is the kinematic viscosity of water.) An excellent coincidence between  $u^*(z^*)$  and the Prandtl-Blasius profile is seen for  $z^* \lesssim 2$ . Whereas the values of  $u(z)$  are clearly lower than those of the Prandtl-Blasius profile in the region around the viscous BL ( $0.7 \lesssim z/\lambda_v \lesssim 2$ ).

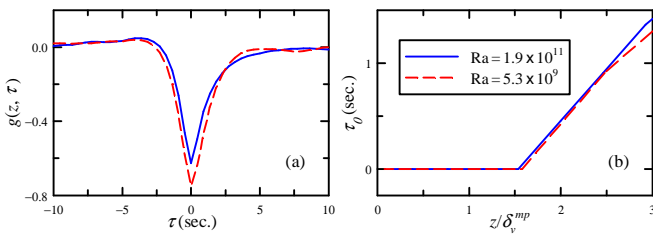


FIG. 4: (color online) (a) Cross-correlation function  $g(z, \tau)$  between  $\delta_v(t)$  and  $u(z, t)$  measured at  $z = 0.76\delta_v^{mp}$ . (b) The normalized peak position  $\tau_0$  as a function of  $z/\delta_v^{mp}$ .

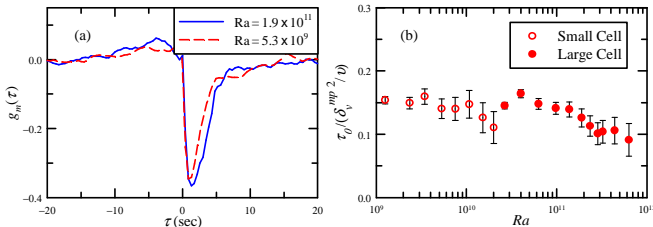


FIG. 5: (color online) (a) Cross-correlation function  $g_m(\tau)$  between  $\delta_v(t)$  and  $u_m(t)$ . (b) The normalized peak position  $\tau_0$  of  $g_m(\tau)$  as a function of  $Ra$ .

With the measured  $\delta_v(t)$ , we can now study some of its dynamic properties and find out what is responsible for its thickness fluctuation. We calculate the cross-correlation function between  $\delta_v(t)$  and  $u(z, t)$ , i.e.,  $g(z, \tau) = \langle [\delta_v(t) - \langle \delta_v(t) \rangle][u(z, t - \tau) - \langle u(z, t) \rangle] \rangle / \sigma_\delta \sigma_u$ , for each measuring vertical position  $z$  and for each  $Ra$ . Here,  $\sigma_\delta = \sqrt{\langle [\delta_v(t) - \langle \delta_v(t) \rangle]^2 \rangle}$ ,  $\sigma_u = \sqrt{\langle [u(z, t) - \langle u(z, t) \rangle]^2 \rangle}$ , and  $\langle \dots \rangle$  denotes a time average. Figure 4(a) shows two examples of  $g(z, \tau)$  measured inside the viscous BL. The presence of a strong negative peak for both correlation functions and the fact that the peaks are located at  $\tau_0 = 0$  suggest that the thinning of the viscous BL and the increasing of  $u(z, t)$  occur simultaneously. We further note that  $\tau_0 = 0$  holds for  $z \lesssim 1.5\delta_v^{mp}$  for all  $Ra$  investigated [see, e.g., Fig. 4(b)] and hence it is a BL property. It is further found that  $\delta_v(t)$  and  $u(z, t)$  are highly correlated inside and around the viscous BL for all measured  $Ra$  [see, e.g., Fig. 4(a)]. This suggests that the fluctuations of horizontal velocity measured locally close to the plate (e.g. at a single point) can be used as an instantaneous measure of the fluctuations of the viscous BL thickness  $\delta_v(t)$ , whereas the measurement of  $\delta_v(t)$  itself would require measuring the entire velocity profile.

From Fig. 4(b) it is seen that for  $z \gtrsim 1.5\delta_v^{mp}$  a positive  $\tau_0$  is obtained, suggesting that the zero-time delay is only a boundary property. This can be made more clearly by examining the cross-correlation function  $g_m(\tau)$  between  $\delta_v(t)$  and  $u_m(t)$ , with the instantaneous maximum velocity as a representative of the magnitude of the mean wind. Figure 5(a) shows  $g_m(\tau)$  as a function of time lag

$\tau$ . Two features are worthy of note: (i) There exists a strong negative correlation between  $\delta_v$  and  $u_m$ , which implies that the larger  $u_m$  is, the smaller  $\delta_v$  becomes; (ii) The negative peak of  $g_m(\tau)$  is located at a positive time lag  $\tau_0$ , indicating that the fluctuations of  $u_m$  leads the variation of  $\delta_v$ . This is because a time delay is needed to transfer the momentum from the mean wind to the interior of the BL. Figure 5(b) shows the  $Ra$ -dependence of the  $\tau_0$ , normalized by the typical timescale  $\delta_v^{mp2}/\nu$  of momentum transfer across the BL via viscosity. It is seen that  $\tau_0/(\delta_v^{mp2}/\nu)$  varies around 0.14 for  $Ra \lesssim 10^{11}$  and decreases slightly with increasing  $Ra$  for  $Ra \gtrsim 10^{11}$ . Here, the decrease of  $\tau_0/(\delta_v^{mp2}/\nu)$  at high Rayleigh numbers suggests an increased contribution from Reynolds stress to the total shear stress inside the BL [11]. Direct study of shear stress around the viscous BL further reveal that Reynolds stress becomes more important than viscous stress for  $Ra \gtrsim 10^{11}$  and hence the BL changes gradually from being laminar to a more turbulent one.

Finally, we check the scaling properties of  $\delta_v(t)$ . We use  $\delta_v^{mp}$  as the typical viscous BL thickness. The best power-law fits give  $\delta_v^{mp}/H \sim 0.64Re^{-0.49 \pm 0.02}$  for the small cell and  $\delta_v^{mp}/H \sim 0.60Re^{-0.51 \pm 0.02}$  for the large cell, where  $Re = [u^*(z^*)]_{max}H/\nu$  is the large-scale Reynolds number. All these results are in line with those obtained using the time-averaged profiles measured in the laboratory frame [11] and the measured  $\delta_v^{mp}/H$ - $Re$  scaling exponents are in good agreement with the theoretical value of  $-0.5$  for the Prandtl-Blasius BL, further confirming the conclusion of the Prandtl-Blasius-type laminar BL in RB system [11, 14].

We thank Chao Sun for providing us the PIV data measured in the small cell. This work was supported by the Research Grants Council of Hong Kong SAR (Nos. CUHK403806 and 403807). Q. Z. thanks supports of Shanghai NSF (No. 09ZR1411200), Chenguang project (No. 09CG41), and RFDP of Ministry of Education of China (No. 20093108120007).

- 
- [1] H. Schlichting and K. Gersten, *Boundary Layer Theory*. (Springer, 8th ed., 2004).
  - [2] G. Ahlers, S. Grossmann, and D. Lohse, *Rev. Mod. Phys.* **81**, 503 (2009); D. Lohse and K.-Q. Xia, *Annu. Rev. Fluid Mech.* **42**, 335 (2010).
  - [3] A. Belmonte, A. Tilgner, and A. Libchaber, *Phys. Rev. Lett.* **70**, 4067 (1993); *Phys. Rev. E* **50**, 269 (1994).
  - [4] Y.-B. Xin, K.-Q. Xia, and P. Tong, *Phys. Rev. Lett.* **77**, 1266 (1996); Y.-B. Xin and K.-Q. Xia, *Phys. Rev. E* **56**, 3010 (1997).
  - [5] A. Naert, T. Segawa, and M. Sano, *Phys. Rev. E* **56**, R1302 (1997).
  - [6] X.-L. Qiu and K.-Q. Xia, *Phys. Rev. E* **58**, 486 (1998); *Phys. Rev. E* **58**, 5816 (1998).
  - [7] R. L. J. Fernandes and R. J. Adrian, *Expl. Thermal Fluid Sci.* **26**, 355 (2002).

- [8] S. Lam *et al.*, Phys. Rev. E **65**, 066306 (2002).
- [9] R. Verzicco and R. Camussi, J. Fluid Mech. **477**, 19 (2003).
- [10] R. du Puits, C. Resagk, and A. Thess, Phys. Rev. Lett. **99**, 234504 (2007).
- [11] C. Sun, Y.-H. Cheung, and K.-Q. Xia, J. Fluid Mech. **605**, 79 (2008).
- [12] K.-Q. Xia, C. Sun, and S.-Q. Zhou, Phys. Rev. E **68**, 066303 (2003).
- [13] W. S. Cleveland and S. J. Devlin, J. Amer. Statist. Assoc. **83**, 596 (1988).
- [14] S. Grossmann and D. Lohse, J. Fluid Mech. **407**, 27 (2000); Phys. Rev. Lett. **86**, 3316 (2001); Phys. Rev. E **66**, 016305 (2002); Phys. Fluids **16**, 4462 (2004).